The Generation of Free Stream Turbulence Intensity and its Effects on Flow Separation Occurring on a Highly Loaded, Low-Pressure Gas Turbine Blade at Low Reynolds Numbers

Tyler M. Pharris, Olivia E. Hirst
Mechanical Engineering Department
Baylor University
Tyler_Pharris@baylor.edu, Olivia_Hirst@baylor.edu

Kenneth W. Van Treuren
Mechanical Engineering Department
Baylor University
Kenneth_Van_Treuren@baylor.edu

Abstract

Current gas turbine engines experience internal fluid temperatures that are beyond the melting point of many components in the engine. The high-pressure turbine solves this problem by cooling the turbine blades with internal air channels and film cooling; however, the low-pressure turbine, which also experiences high temperatures, does not utilize cooling technologies. The higher temperatures now seen by the low-pressure turbine blade are combined with flow separating from the surface of the blades, resulting in thermal fatigue. At the high Reynolds numbers seen at takeoff, the flow over low-pressure turbine blades tends to stay attached. However, at lower Reynolds numbers (25,000 to 200,000), such as those seen during cruise at high altitudes, the flow on the suction surface of the low-pressure turbine blades can separate. This paper examines how the flow field over the L1A turbine blade varies with a change in low Reynolds numbers (60,000, 108,000, and 165,000) and turbulence intensities (1.89% to 19.87%) within the Baylor University Cascade Wind Tunnel (BUC). Quantifying the change in separated flow seen due to varying Reynolds numbers and turbulence intensities will help to characterize the different flow conditions in the low-pressure turbine and how these changes affect the efficiencies of the engine. The ultimate goal of this research is to improve blade design in the low-pressure turbine for all commercial and military aircraft.

Introduction and Theory

In a turbofan engine, the low-pressure turbine (Fig. 1) is used to extract energy from the flow of a high-pressure, high energy fluid and convert the extracted energy into work. The engine then uses that work to spin the fan and low-pressure compressor (Fig. 1). Any excess energy not extracted can then be converted into thrust. Therefore, using less energy from the flow to spin the fan and compressor will result in more thrust from the same amount of fuel, thus, producing a more efficient engine.

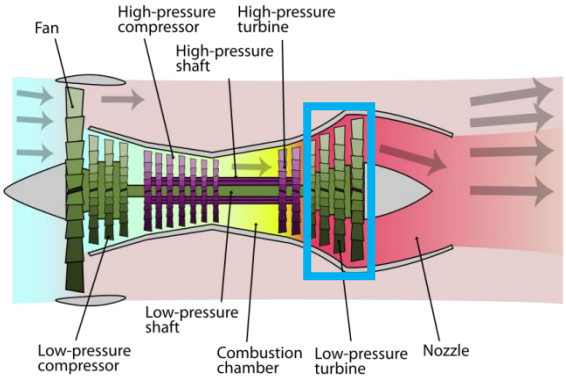

Fig. 1: High Bypass Ratio Turbofan with blue box denoting the low-pressure turbine [1]

Research conducted at NASA Glenn Research Center showed a 2% decrease in the relative efficiency of aircraft engines operating at cruising altitudes when compared to the same engines running at sea level [2]. This decrease in relative efficiency at altitude was found to be mainly caused by flow separation occurring in the low-pressure turbine. When flying at high altitudes, flow separation, which causes pressure losses and lowers efficiencies, can be seen on the suction side of the low-pressure turbine blades. Flow separation occurs when a viscous boundary layer lifts off of the surface of an airfoil due to adverse pressure gradients or sudden turns, both of which are present in the low-pressure turbine. As the flow reaches the maximum thickness of the turbine blade, the air will meet an adverse pressure gradient which causes the air to decelerate. When the airflow does not have the momentum needed to overcome the adverse pressure gradient, the boundary layer will separate, resulting in less usable work. Effectively, flow separation reduces the overall efficiency of the engine.

Flow separation is very common at high altitudes because there is a lower air density than at sea level. For example, at a cruise altitude of 60,000 feet, the density of air drops to one-tenth of that seen at sea level. Such a low air density along with a low cruising speed can result in a reduced Reynolds number (Re) typically between 25,000 and 200,000. Reynolds number (Equation 1) is defined as the product of the density of the fluid, ρ, velocity of the fluid, V, and the characteristic length of the airfoil, c, all divided by the dynamic viscosity of the fluid, μ:

$$\mathrm{Re} = \frac{\rho V c}{\mu} = \frac{\text{Inertia Forces}}{\text{Viscous Forces}} \tag{1}$$

The Reynolds number can also be thought of as the ratio comparing the inertia forces in the flow to the viscous forces between the fluid and the airfoil. Because the density of the air has fallen, the Reynolds number is smaller; therefore, there is less momentum in the flow. This means the flow no longer has the inertia needed to stay attached to the turbine blades, thus, the flow separates under the influence of the adverse pressure gradient and turn.

Previous studies have presented research showing the Reynolds number and free stream turbulence intensity (FSTI) affects not only the size, but also the location of the separation

bubble on the suction surface of turbine blades [3]. This paper seeks to examine the research previously conducted as well as investigate and quantify the effects that varying the Reynolds number and FSTI have on the separation bubble size and location.

Apparatus and Experimental Procedure

Apparatus

The experimental apparatus centers on the BUC and its ability to simulate very low momentum flows, similar to those seen in the low-pressure turbine at cruising altitudes. The BUC is an open-circuit, cascade wind tunnel designed to provide steady, slow flows over a series of L1A model low-pressure turbine vanes. The BUC consists of a blower type fan, data acquisition (DAQ) system, computer, two digital sensor arrays, a differential pressure transducer, a pitot-static tube, constant temperature hotwire anemometer, and 5 L1A model low-pressure turbine vanes (Fig. 2).

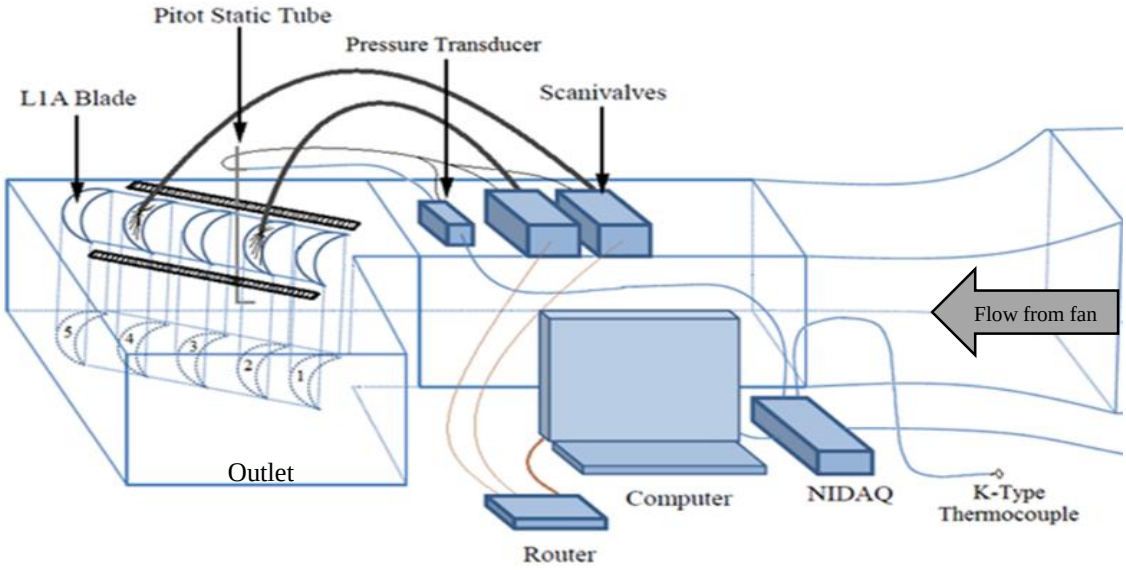

Fig. 2: BUC Schematic [4]

The blower type fan, a Cincinnati Blower Fan model HDBI-160, provides the pressure gradient needed to blow air at specified speeds through the BUC. The total and static pressure of the flow upstream of the test section is measured with a pitot-static tube and pressure tubing that is connected to a Mamac Systems PR-274 pressure transducer. The differential pressure transducer then measures the dynamic pressure and sends the data to the DAQ system. The dynamic pressure is expressed in Equation 2, where P_T is the total pressure, P_S is the static pressure upstream of the test section, ρ represents the density of the air, and V is the downstream velocity:

$$P_T - P_S = \frac{1}{2}\rho V^2 \tag{2}$$

The DAQ system consists of a NI 9211 Thermocouple Input Card, NI 9205 Analog Input Card, and a NI 9263 Analog Output Card which are all housed inside of a NI compact DAQ 9172 chassis. The NI 9211 Thermocouple Input Card reads the temperature of the ambient air measured by a K-type thermocouple located just outside of the cascade tunnel. The NI 9205 Analog Input Card takes differential pressure data in voltage form from the Mamac Systems PR-274 pressure transducer. The NI 9263 Analog Output Card controls the test section Reynolds number by sending a voltage to the Cincinnati Blower Fan, read with the pitot-static tube. Each DAQ card is controlled by the NI compact DAQ 9172 chassis which coordinates data transfer between a NI LabVIEW code and the DAQ cards.

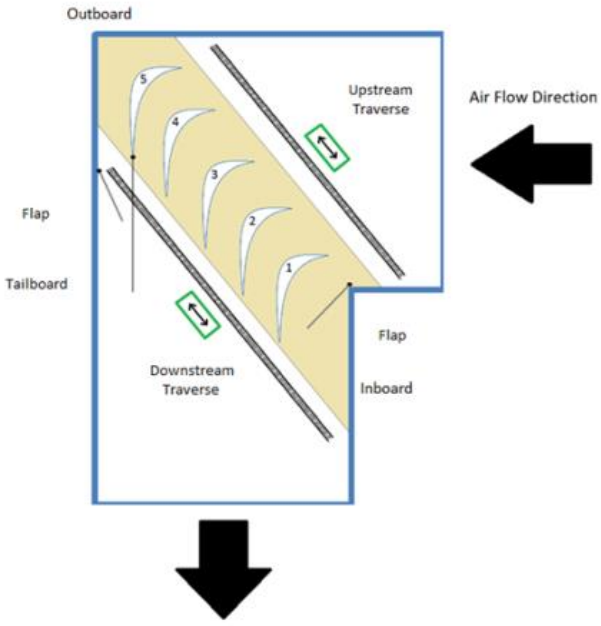

Fig. 3: Baylor University Cascade research wind tunnel test section [4]

Five test blades with the L1A blade profile make up the BUC test section. The five blades are set at a 35 degree inlet angle and a 60 degree outlet angle. This provides an offset angle of 5% at the outlet of the test section. Blades one, three, and five (numbered right to left in Fig. 3) were fabricated using a Dimension SST 768 3D printer. Blades two and four were fabricated using stereolithography and each has a total of 41 pressure ports – 21 on the suction surface, 20 on the pressure surface. Through tubing, the pressure ports are connected to two Scanivalve Digital Sensor Array 3217s (DSAs) which use the blades to measure the static pressure on the surfaces of the blade at the ports (Fig. 4). Data from the DSAs is acquired and stored using the LabVIEW code.

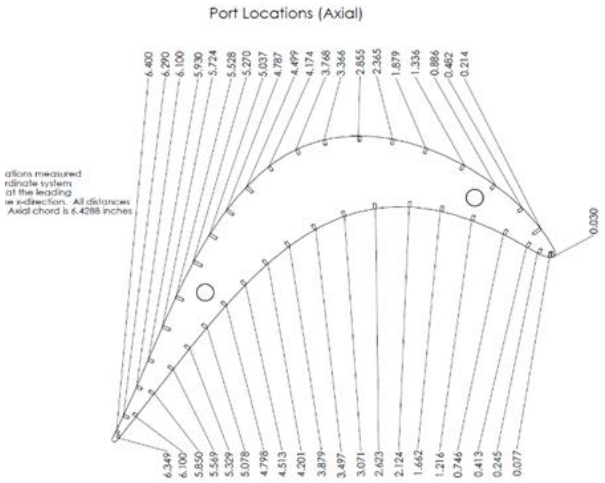

Fig. 4: Pressure ports on surface of L1A blade in relation to axial chord [5]

The pressure distribution over the blades is mapped using the coefficient of pressure, C_p. The coefficient of pressure is a dimensionless number that relates the velocity of the flow over the test blade at the normalized distance along the suction surface length. The coefficient of pressure is expressed in Equation 3, where the total pressure measured upstream of the test section (P_T) is subtracted by the static pressure measured at each pressure port ($P_{S_{local}}$) and divided by the dynamic head (Equation 2):

$$C_p = \frac{P_T - P_{S_{local}}}{\frac{1}{2}\rho V^2} = \frac{P_T - P_{S_{local}}}{P_T - P_S} \tag{3}$$

Additionally, a constant temperature hotwire anemometer and two traverses were used to determine the FSTI in the BUC. The hotwire setup includes an IFA 300 constant temperature anemometer system and a single wire hotwire probe located just upstream of the test section. The BUC's two traverses, one upstream and one downstream, were run by the LabVIEW code. The upstream traverse holds the pitot-static tube used to measure the upstream total pressure, upstream static pressure, upstream dynamic pressure, and ultimately velocity in the tunnel.

Experimental Procedure

Turbulence Sweep Tests

The turbulence intensity was measured using the IFA 300 with a single hotwire anemometer attached to and above the pitot-static tube. The hotwire was oriented parallel to the floor and ceiling of the tunnel and faced directly into the flow from the fan. The hotwire was moved via the upstream traverse. FSTIs were recorded at half-inch increments across a 19.5 inch span over the entirety of the cascade test section, resulting in 40 points where the FSTI was measured. After each test the turbulence intensity measured by the hotwire was recorded by hand into Excel and put into graph format for visualization and simplified analysis. The FSTIs are then averaged over the span and result in a general FSTI for each test.

Turbulence tests were run at Reynolds numbers of approximately 60,000, 108,000, and 165,000. At each of these Reynolds numbers, turbulence tests were run under five different conditions: a "clean tunnel" configuration using no turbulence grid and with a variety of "dirty tunnel" configurations utilizing wood turbulence grids of sizes 0.5 inch, 0.75 inch, 1.0 inch, and 1.5 inches. The construction of these grids was based on a square mesh array of square bars, utilizing a similar design to that which was categorized by Roach [6] with a goal of resulting turbulence intensities from the grids to vary between 3% and 20%. A significant adjustment that separates our resulting turbulences from accurately matching that predicted by Roach is that while the first row of bars that the flow encounters is square-mesh-square (SMS), the second row of bars has a slightly altered design. The second row of bars, which run perpendicular to the first row of bars, is the same height and width as suggested by Roach; however, the thickness of the second row for all grids is 0.5 inch due to the BUC's grid holder restrictions.

C_p Tests

The pressure variations along the surfaces of the turbine blades are mapped by calculating the C_p seen at each of the static pressure port locations along blades 2 and 4 (Equation 3) and then plotting. The total pressure, P_T, is measured in the stagnation tube on the pitot-static probe, the static pressure, P_S, is measured on the static pressure ports on the outside of the probe, and the local static pressure, $P_{S_{local}}$, is measured at each of the 41 pressure ports of blades 2 and 4.

C_p tests were also run at Reynolds numbers of approximately 60,000, 108,000, and 165,000. At each Reynolds number, tests were run under five different turbulence conditions: with the "clean tunnel" configuration and each of the four "dirty tunnel" configurations for a total of 15 C_p tests. The grids used for the C_p tests were the same as those utilized in the turbulence sweep tests. The C_p plots allow the data to be used to visually and quantitatively analyze the flow characteristics seen on the blades at varying Reynolds numbers and FSTIs.

Results

With five different FSTIs and three different Reynolds numbers available, a turbulence sweep test and a C_p test was taken at each of the 15 conditions. Each test used a Reynolds number of 60,000, 108,000, or 165,000 as an approximate testing point. The fan was then operated at a speed that produced an average Reynolds number in the test section near the three desired Reynolds numbers. Each of these test speeds was then run under a different turbulence condition by interchanging the four turbulence grids with the clean tunnel configuration to complete the matrix (Table 1).

Table 1: Test Matrix

Test Matrix	Clean Configuration: No Turbulence Grid	Dirty Configuration: 0.5 Inch SMSR Turb. Grid	Dirty Configuration: 0.75 Inch SMSR Turb. Grid	Dirty Configuration: 1.0 Inch SMSR Turb. Grid	Dirty Configuration: 1.5 Inch SMSR Turb. Grid
Reynolds Number: 60000	**Test 1**: Reynolds Number: 61742; FSTI: 1.89%	**Test 4**: Reynolds Number: 60645; FSTI: 3.12%	**Test 7**: Reynolds Number: 59233; FSTI: 6.26%	**Test 10**: Reynolds Number: 61666; FSTI: 9.39%	**Test 13**: Reynolds Number: 60236; FSTI: 15.26%
Reynolds Number: 108000	**Test 2**: Reynolds Number: 110525; FSTI: 2.82%	**Test 5**: Reynolds Number: 109550; FSTI: 4.24%	**Test 8**: Reynolds Number: 107857; FSTI: 7.78%	**Test 11**: Reynolds Number: 108605; FSTI: 11.92%	**Test 14**: Reynolds Number: 105722; FSTI: 19.28%
Reynolds Number: 165000	**Test 3**: Reynolds Number: 164910; FSTI: 3.60%	**Test 6**: Reynolds Number: 167528; FSTI: 4.76%	**Test 9**: Reynolds Number: 164713; FSTI: 8.66%	**Test 12**: Reynolds Number: 164551; FSTI: 13.18%	**Test 15**: Reynolds Number: 162708; FSTI: 19.87%

Turbulence Sweep Tests

Figures 5 and 6 consist of graphs that help with visualizing and analyzing the results of the turbulence sweep tests for each of the 15 different conditions. These graphs show how the FSTI fluctuates at various points across the test section just upstream of the blades.

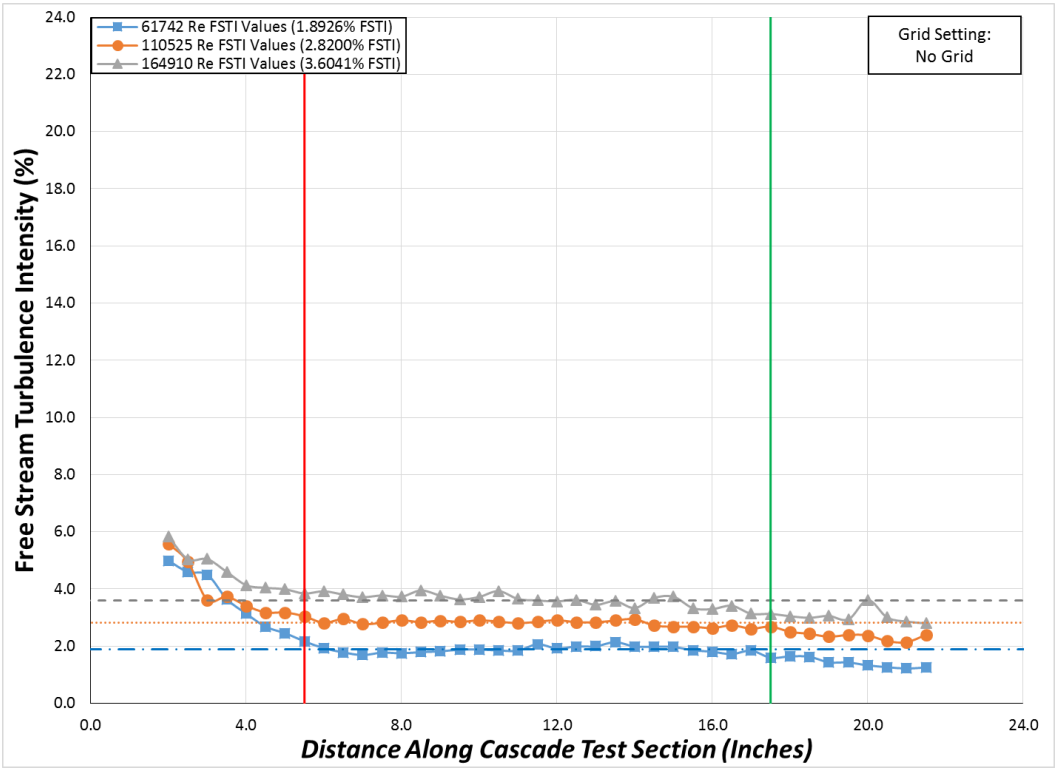

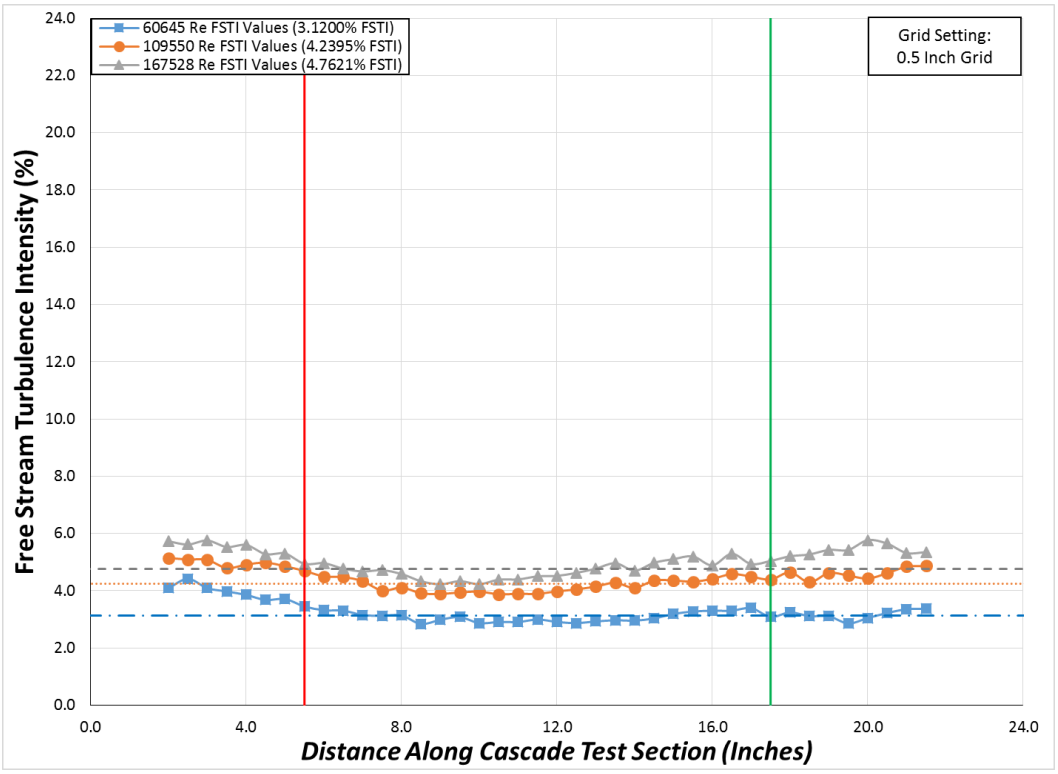
60645 Re FSTI Values (3.1200% FSTI)
109550 Re FSTI Values (4.2395% FSTI)
167528 Re FSTI Values (4.7621% FSTI)
Grid Setting:
0.5 Inch Grid
Free Stream Turbulence Intensity (%)
Distance Along Cascade Test Section (Inches)
0.0
2.0
4.0
6.0
8.0
10.0
12.0
14.0
16.0
18.0
20.0
22.0
24.0

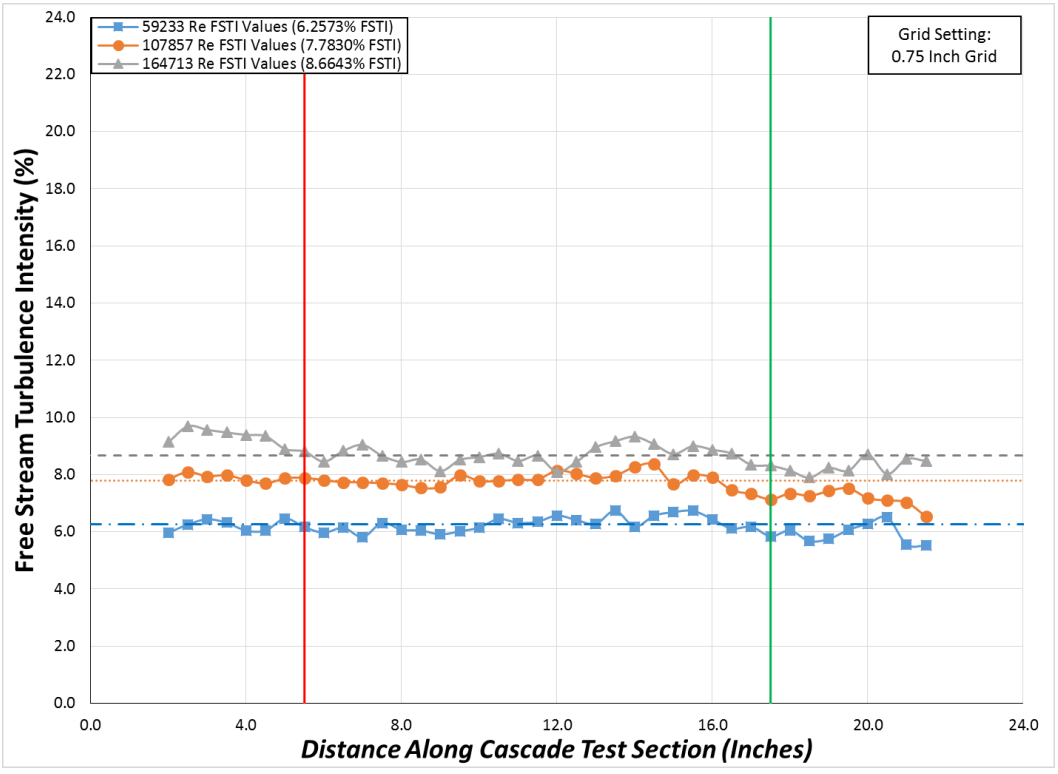
59233 Re FSTI Values (6.2573% FSTI)
107857 Re FSTI Values (7.7830% FSTI)
164713 Re FSTI Values (8.6643% FSTI)
Grid Setting:
0.75 Inch Grid
Free Stream Turbulence Intensity (%)
Distance Along Cascade Test Section (Inches)
0.0
2.0
4.0
6.0
8.0
10.0
12.0
14.0
16.0
18.0
20.0
22.0
24.0

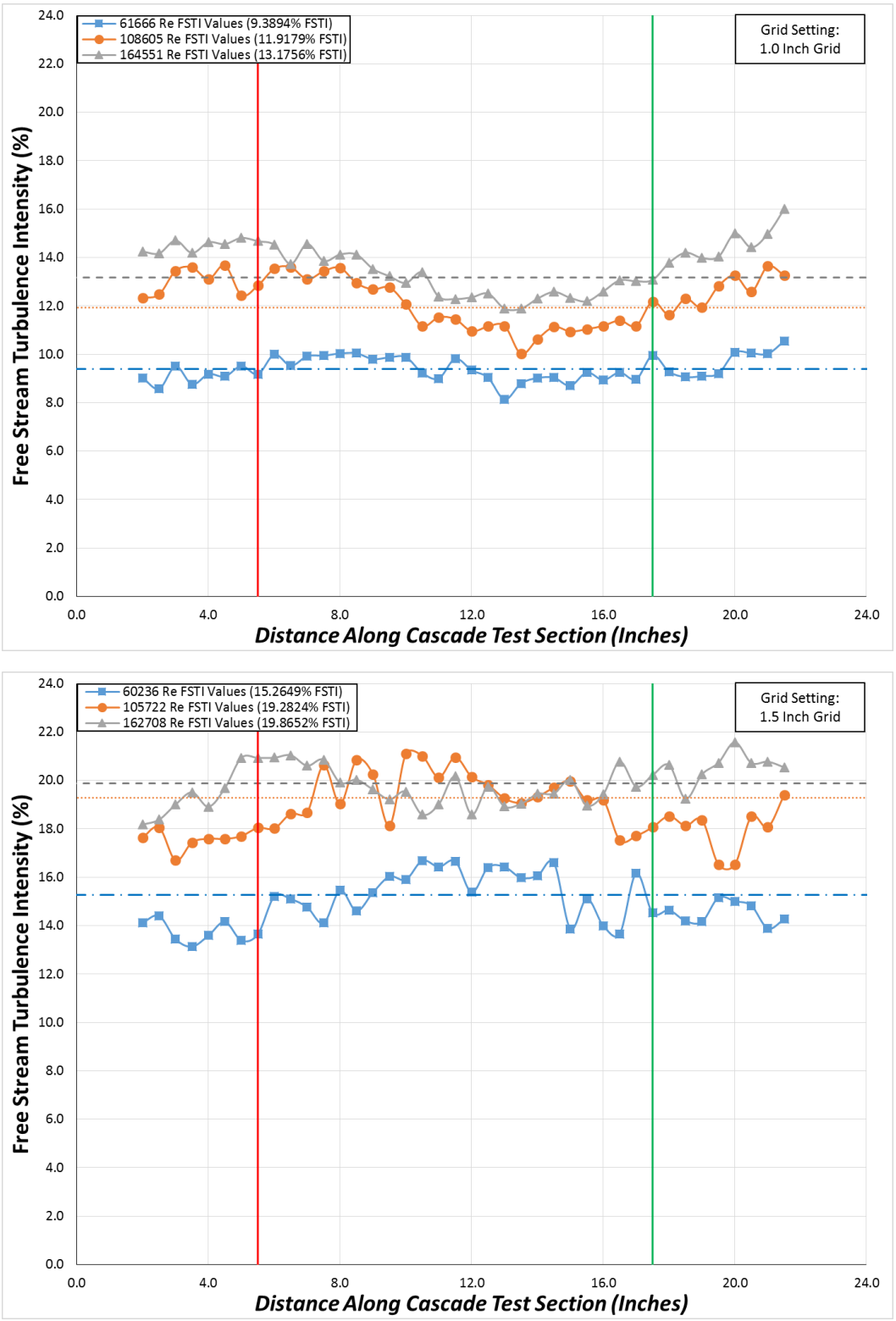

Fig. 5: Turbulence Sweep Tests Using the Same Grid while Varying Reynolds Number: Read Top to Bottom - *FSTI Graph with No Grid, FSTI Graph with 0.5 Inch Grid, FSTI Graph with 0.75 Inch Grid, FSTI Graph with 1.0 Inch Grid, FSTI Graph with 1.5 Inch Grid*

Figure 5 shows one view of the results from the turbulence sweep tests. Each graph represents a different clean tunnel/dirty tunnel configuration for a total of 5 graphs. In each graph are the FSTIs found at 60,000, 108,000, and 165,000 Re – both in 0.5 inch increments across the BUC and averaged across blades 2 and 4. Each of the graphs show the results of the turbulence sweep tests by plotting the FSTI on the y-axis and the location in the cascade test section on the x-axis.

Table 2: Average FSTI under each of the 15 possible conditions

Test Matrix	Clean Configuration: No Turbulence Grid	Dirty Configuration: 0.5 Inch SMSR Turb. Grid	Dirty Configuration: 0.75 Inch SMSR Turb. Grid	Dirty Configuration: 1.0 Inch SMSR Turb. Grid	Dirty Configuration: 1.5 Inch SMSR Turb. Grid
Reynolds Number: 60000	FSTI: 1.89%	FSTI: 3.12%	FSTI: 6.26%	FSTI: 9.39%	FSTI: 15.26%
Reynolds Number: 108000	FSTI: 2.82%	FSTI: 4.24%	FSTI: 7.78%	FSTI: 11.92%	FSTI: 19.28%
Reynolds Number: 165000	FSTI: 3.60%	FSTI: 4.76%	FSTI: 8.66%	FSTI: 13.18%	FSTI: 19.87%

The comparisons in Figure 5 show the effect that altering the Reynolds number and keeping the same grid have on the FSTI in the BUC. After conducting turbulence sweep tests under each of the 15 test conditions, two trends have been shown in the results. First, as the Reynolds number in the test section increased, the average FSTI increased as well. Table 2 shows that as the Reynolds number increased from 60,000 to 108,000, the FSTI increased, and as the Reynolds number increased from 108,000 to 165,000, the FSTI increased again. This trend is shown for the clean configuration of the tunnel as well as each of the dirty configurations. It was also shown each time the turbulence grids remained constant, and the Reynolds number varied. Second, in each of the five comparisons, FSTI in the tunnel increased faster between 60,000 to 108,000 Re then it did when changing the Reynolds number from 108,000 to 165,000 (Table 3). This trend is shown for the clean configuration of the tunnel as well as each of the dirty configurations.

Table 3: FSTI changes as Reynolds number changes

Test Matrix	Clean Configuration: No Turbulence Grid	Dirty Configuration: 0.5 Inch SMSR Turb. Grid	Dirty Configuration: 0.75 Inch SMSR Turb. Grid	Dirty Configuration: 1.0 Inch SMSR Turb. Grid	Dirty Configuration: 1.5 Inch SMSR Turb. Grid
Reynolds Number Change: 60000 to 108000	FSTI Change: 0.93%	FSTI Change: 1.12%	FSTI Change: 1.53%	FSTI Change: 2.53%	FSTI Change: 4.02%
Reynolds Number Change: 108000 to 165000	FSTI Change: 0.78%	FSTI Change: 0.52%	FSTI Change: 0.88%	FSTI Change: 1.26%	FSTI Change: 0.58%

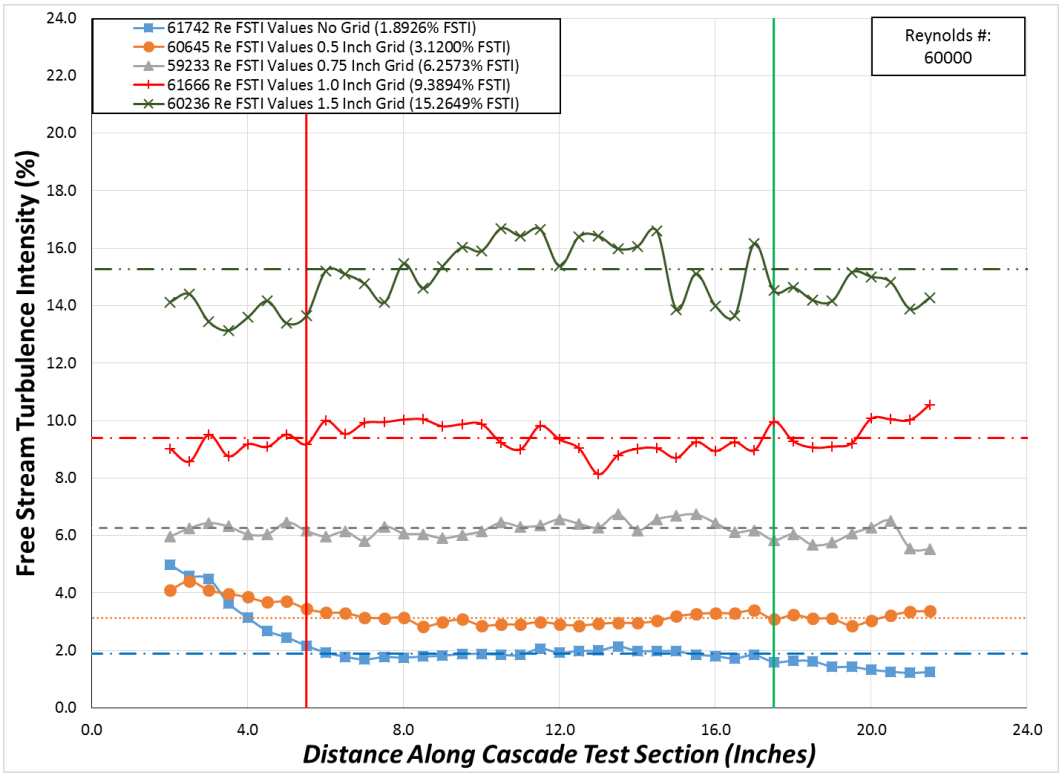
61742 Re FSTI Values No Grid (1.8926% FSTI)
60645 Re FSTI Values 0.5 Inch Grid (3.1200% FSTI)
59233 Re FSTI Values 0.75 Inch Grid (6.2573% FSTI)
61666 Re FSTI Values 1.0 Inch Grid (9.3894% FSTI)
60236 Re FSTI Values 1.5 Inch Grid (15.2649% FSTI)
Reynolds #: 60000
Free Stream Turbulence Intensity (%)
Distance Along Cascade Test Section (Inches)
0.0
2.0
4.0
6.0
8.0
10.0
12.0
14.0
16.0
18.0
20.0
22.0
24.0

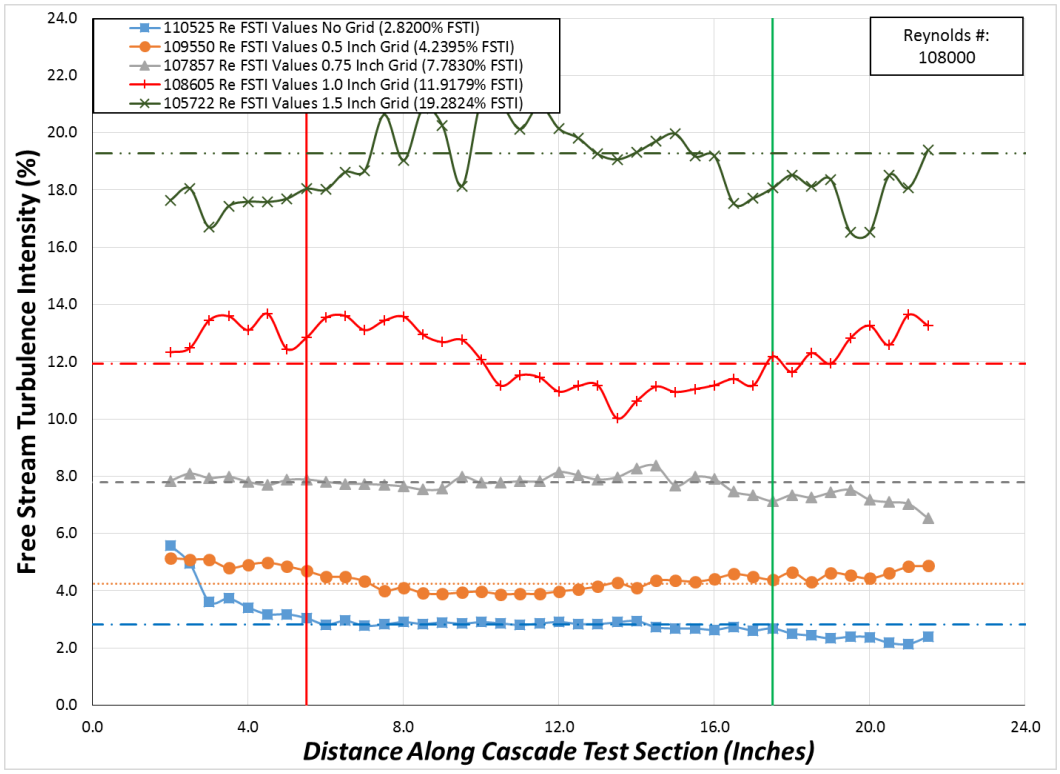
110525 Re FSTI Values No Grid (2.8200% FSTI)
109550 Re FSTI Values 0.5 Inch Grid (4.2395% FSTI)
107857 Re FSTI Values 0.75 Inch Grid (7.7830% FSTI)
108605 Re FSTI Values 1.0 Inch Grid (11.9179% FSTI)
105722 Re FSTI Values 1.5 Inch Grid (19.2824% FSTI)
Reynolds #: 108000
Free Stream Turbulence Intensity (%)
Distance Along Cascade Test Section (Inches)
0.0
2.0
4.0
6.0
8.0
10.0
12.0
14.0
16.0
18.0
20.0
22.0
24.0

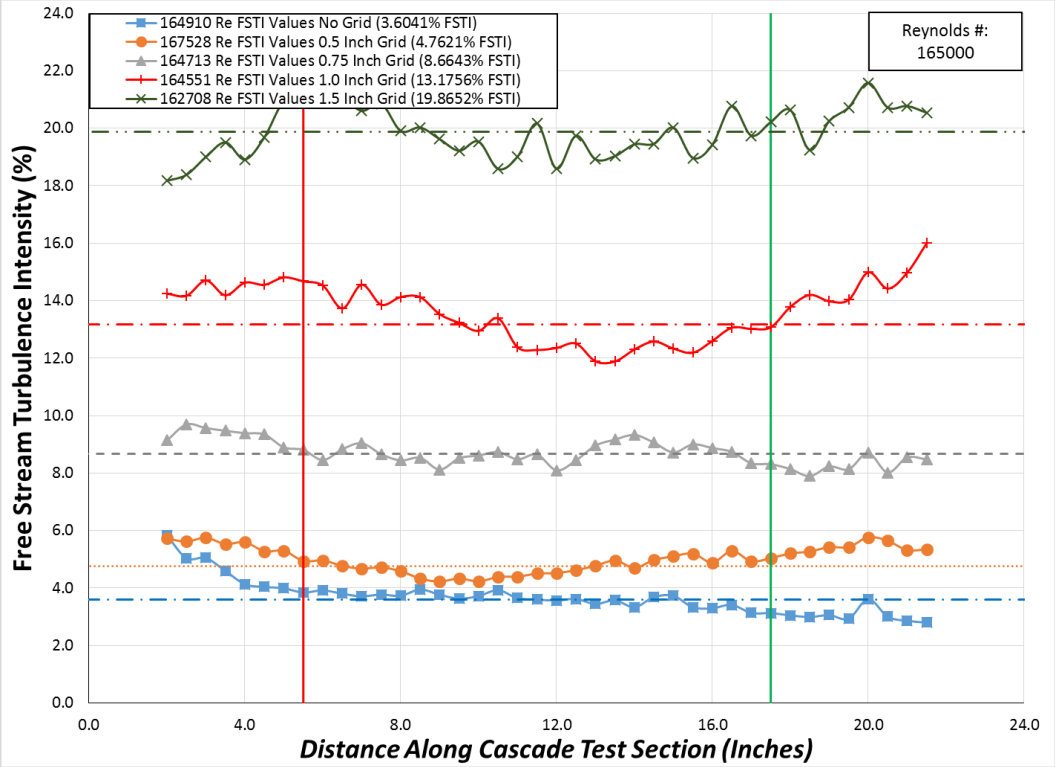

Fig. 6: Turbulence Sweep Tests Using the Same Reynolds Number while Varying Grid Sizes: Read Top to Bottom - *FSTI Graph of 60,000 Re, FSTI Graph at 108,000 Re, and FSTI Graph at 165,000 Re*

Figure 6 shows another view of the results from the turbulence sweep tests. Each graph represents a different Reynolds number (60,000, 108,000, and 165,000) for a total of 3 graphs. In each graph are the FSTIs found under each of the 5 clean tunnel/dirty tunnel configurations – both in 0.5 inch increments across the BUC and averaged across blades 2 and 4. Each of the graphs show the results of the turbulence sweep tests by plotting the FSTI on the y-axis and the location in the cascade test section on the x-axis.

Table 2 shows the average FSTIs found for 60,000, 108,000, and 165,000 Re. These 3 comparisons analyze the difference that altering grid size has on the FSTI in the cascade when using the same Reynolds number. However, there are no large trends visible when using the comparisons in Figure 6.

Coefficient of Pressure Tests

Figures 7 and 8 consist of graphs that help with visualizing and analyzing the results obtained when running C_p tests for each of the 15 different conditions. These graphs show how the C_p fluctuates at various points along the suction surfaces of the blades.

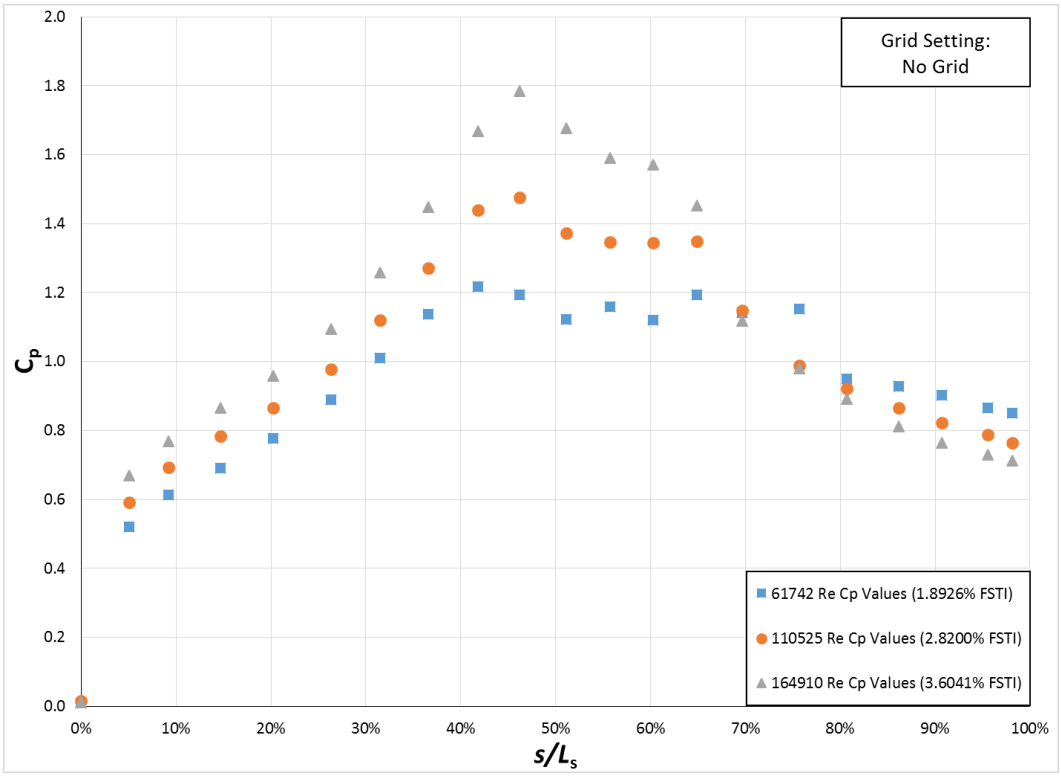
Grid Setting:
No Grid
61742 Re Cp Values (1.8926% FSTI)
110525 Re Cp Values (2.8200% FSTI)
164910 Re Cp Values (3.6041% FSTI)
C_p
s/L_s
0.0
0.2
0.4
0.6
0.8
1.0
1.2
1.4
1.6
1.8
2.0
0%
10%
20%
30%
40%
50%
60%
70%
80%
90%
100%

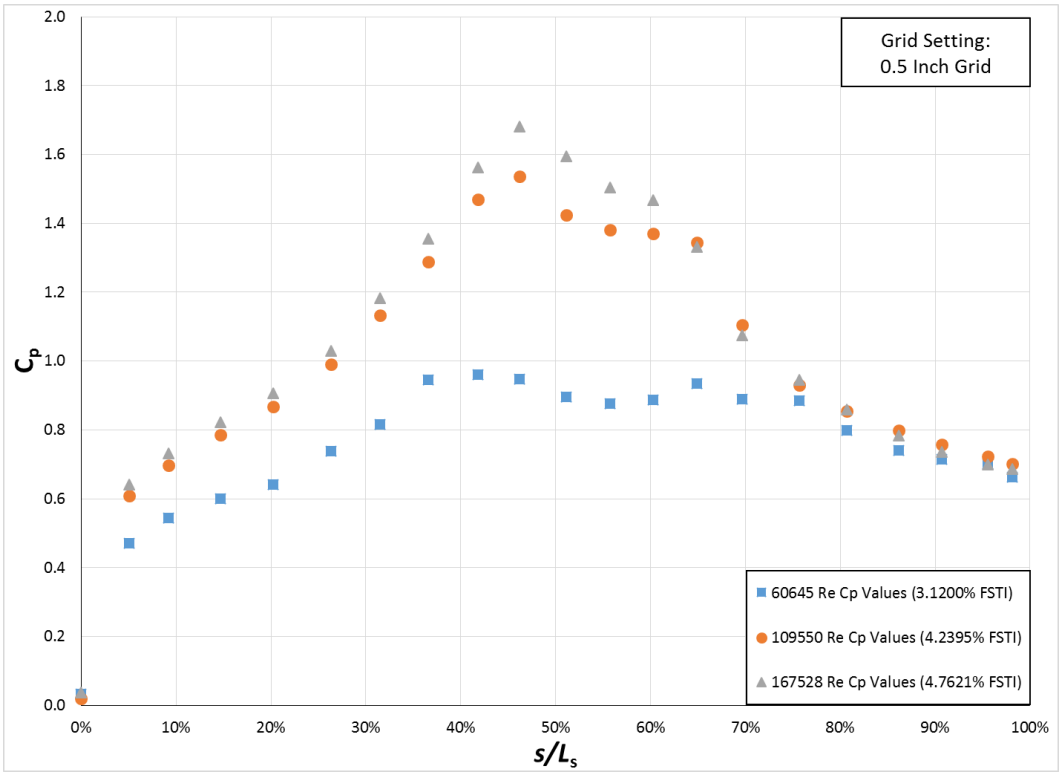
Grid Setting:
0.5 Inch Grid
60645 Re Cp Values (3.1200% FSTI)
109550 Re Cp Values (4.2395% FSTI)
167528 Re Cp Values (4.7621% FSTI)
C_p
s/L_s
0.0
0.2
0.4
0.6
0.8
1.0
1.2
1.4
1.6
1.8
2.0
0%
10%
20%
30%
40%
50%
60%
70%
80%
90%
100%

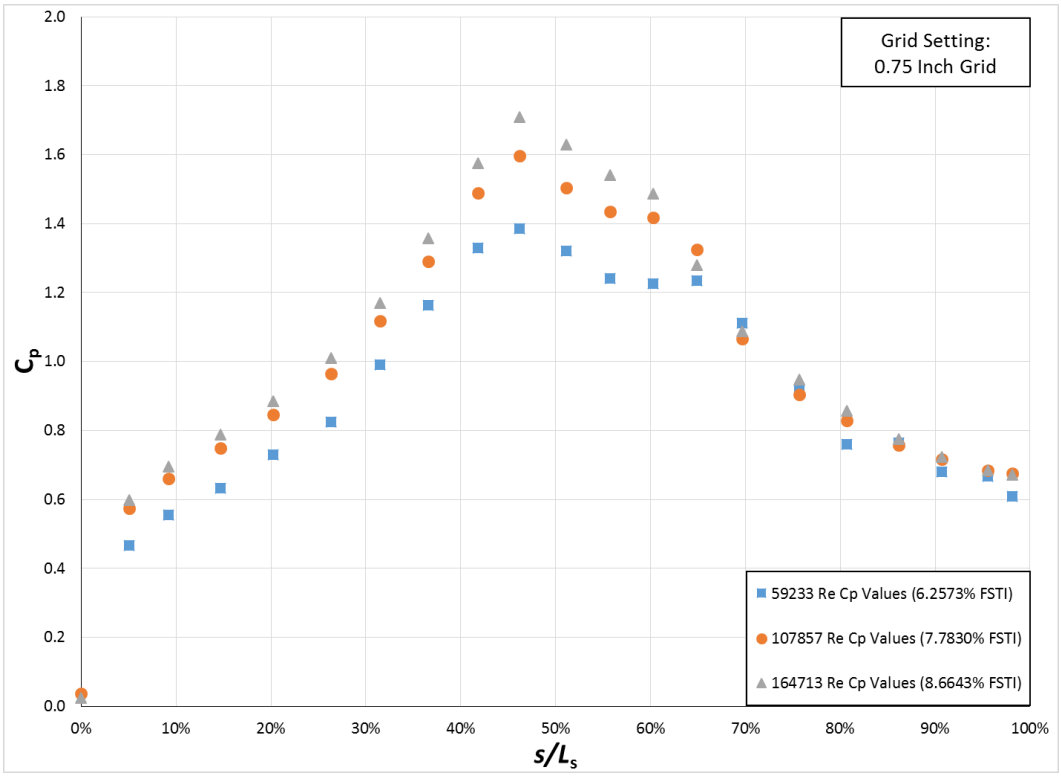
Grid Setting:
0.75 Inch Grid
59233 Re Cp Values (6.2573% FSTI)
107857 Re Cp Values (7.7830% FSTI)
164713 Re Cp Values (8.6643% FSTI)
C_p
s/L_s
2.0
1.8
1.6
1.4
1.2
1.0
0.8
0.6
0.4
0.2
0.0
0%
10%
20%
30%
40%
50%
60%
70%
80%
90%
100%

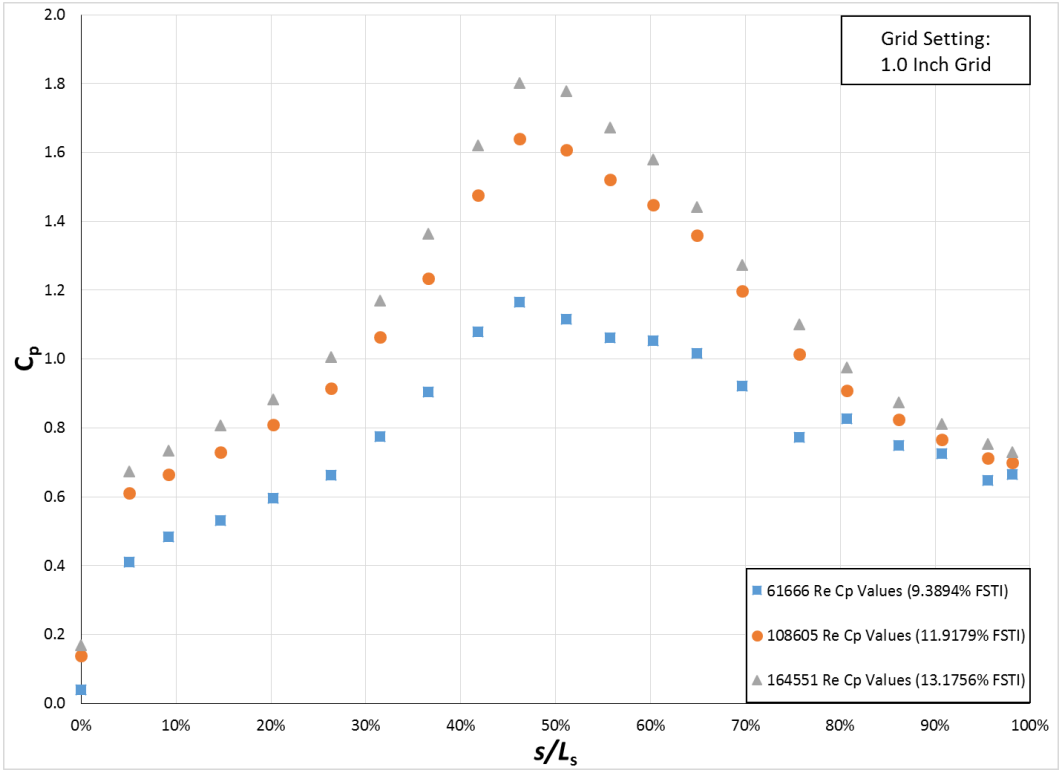
Grid Setting:
1.0 Inch Grid
61666 Re Cp Values (9.3894% FSTI)
108605 Re Cp Values (11.9179% FSTI)
164551 Re Cp Values (13.1756% FSTI)
C_p
s/L_s
2.0
1.8
1.6
1.4
1.2
1.0
0.8
0.6
0.4
0.2
0.0
0%
10%
20%
30%
40%
50%
60%
70%
80%
90%
100%

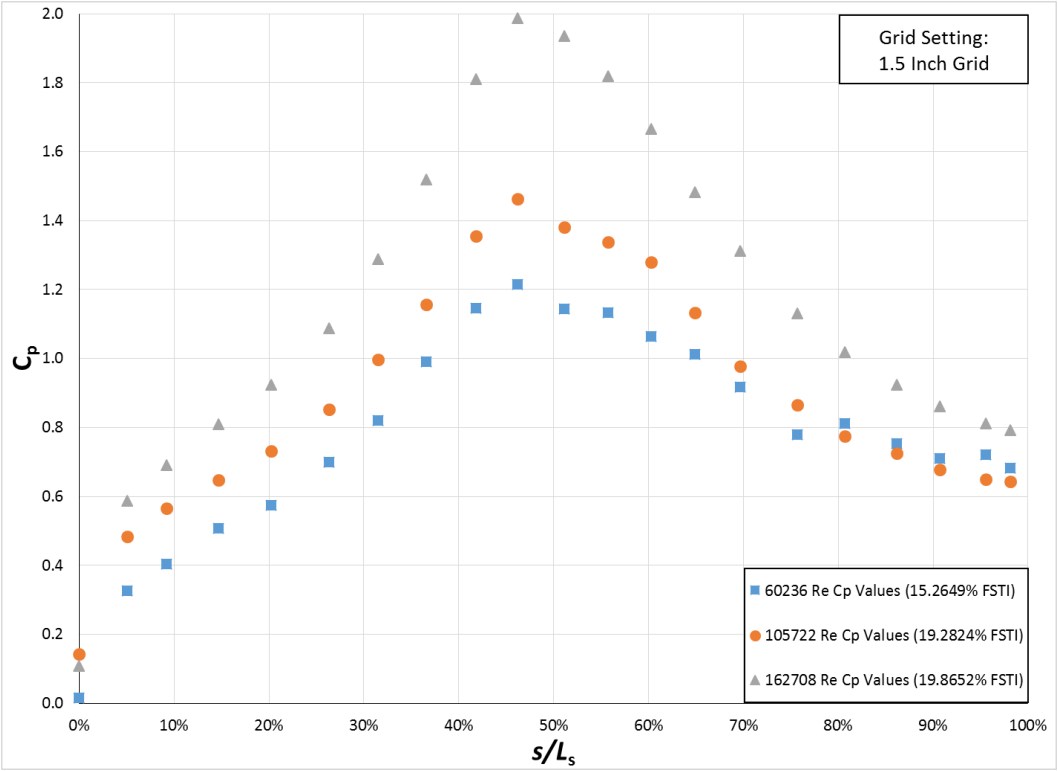

Fig. 7: Coefficient of Pressure Tests Using the Same Grid while Varying Reynolds Number: Read Top to Bottom - *C_p Graph with No Grid, C_p Graph with 0.5 Inch Grid, C_p Graph with 0.75 Inch Grid, C_p Graph with 1.0 Inch Grid, C_p Graph with 1.5 Inch Grid*

Figure 7 shows the C_p tests when using the same turbulence grid in the tunnel but varying the Reynolds number present in the test section. Each graph represents a different clean tunnel/dirty tunnel configuration. The markers represent the C_p's calculated at the 21 pressure ports along the suction surface of the inboard blade. Each of these comparisons show the results of the pressure variations along the blades. The C_p is plotted on the y-axis and the normalized position with respect to the suction surface length, s, is plotted on the x-axis.

Table 4: Reynolds Number, FSTI, and Interpolated Separation Locations for all 15 Tests

Test Matrix	**Clean Configuration: No Turbulence Grid**	**Dirty Configuration: 0.5 Inch SMSR Turb. Grid**	**Dirty Configuration: 0.75 Inch SMSR Turb. Grid**	**Dirty Configuration: 1.0 Inch SMSR Turb. Grid**	**Dirty Configuration: 1.5 Inch SMSR Turb. Grid**
Reynolds Number: 60000	Reynolds Number: 61742 FSTI: 1.89% Separation Location: 39.67%	Reynolds Number: 60645 FSTI: 3.12% Separation Location: 37.13%	Reynolds Number: 59233 FSTI: 6.26% Separation Location: 51.92%	Reynolds Number: 61666 FSTI: 9.39% Separation Location: 51.64%	Reynolds Number: 60236 FSTI: 15.26% Separation Location: 51.13%
Reynolds Number: 108000	Reynolds Number: 110525 FSTI: 2.82% Separation Location: 51.36%	Reynolds Number: 109550 FSTI: 4.24% Separation Location: 51.42%	Reynolds Number: 107857 FSTI: 7.78% Separation Location: 56.80%	Reynolds Number: 108605 FSTI: 11.92% Separation Location: 64.86%	Reynolds Number: 105772 FSTI: 19.28% Separation Location: 60.31%
Reynolds Number: 165000	Reynolds Number: 164910 FSTI: 3.60% Separation Location: 56.80%	Reynolds Number: 167528 FSTI: 4.76% Separation Location: 57.54%	Reynolds Number: 164713 FSTI: 8.66% Separation Location: 58.40%	Reynolds Number: 164551 FSTI: 13.18% Separation Location: N/A	Reynolds Number: 162708 FSTI: 19.87% Separation Location: N/A

The graphs in Figure 7 show the difference that altering the Reynolds number has on the coefficients of pressure in the cascade while using the same grid. After conducting the C_p tests for each of the 15 test conditions and comparing the results, several trends have been shown.

First, as the Reynolds number in the test section increased, the separation point moved towards the trailing edge. The separation point is defined as the location where the C_p stops rising or falling and proceeds to plateau. Table 4 shows that as the Reynolds number increases from 60,000 to 108,000 the boundary layer stays attached longer and as the Reynolds number increases from 108,000 to 165,000 the separation point moves even farther downstream. This is shown for the clean configuration of the tunnel as well as each of the dirty configurations. The trend was found each time the turbulence grids remained constant, and the Reynolds number varied. Second, as the FSTI in the tunnel increased, the separation location moved farther down the suction surface of the blade. Reading Table 4 from the left to right on the same row, the Reynolds number is held steady. It is shown that in almost every case an increase in FSTI delays separation.

There are a couple of anomalies present at either the high turbulence or 60,000 Re cases. First, when comparing data between the tests at Reynolds numbers of approximately 60,000, there is an anomaly in the data between the test using no grid and the test using the 0.5 inch grid. The anomaly is seen again between the test using the 0.75 inch grid and the test using the 1.0 inch grid. Ultimately, the anomaly is seen between the test using the 1.0 inch grid and the test using the 1.5 inch grid. Each of these anomalies showed that an increase in FSTI leads to a slightly reduced separation location. This is believed to be caused by surging sometimes experienced in the test section at lower Reynolds numbers. The second anomaly can be seen when comparing data at the higher turbulence cases. The data between the test using the 1.0 inch grid at a Reynolds number of 108,000 and the test using the 1.5 inch grid at a Reynolds number of 108,000. In this case, as the FSTI increased, the separation point decreases. This is believed to be the result of not having enough duct length for large vortices created by the turbulence grid to dissipate before reaching the test section and the result of the large turbulence intensity.

Table 5: Reynolds Number, FSTI, and Max Reattachment Points for all 15 tests

Test Matrix	Clean Configuration: No Turbulence Grid	Dirty Configuration: 0.5 Inch SMSR Turb. Grid	Dirty Configuration: 0.75 Inch SMSR Turb. Grid	Dirty Configuration: 1.0 Inch SMSR Turb. Grid	Dirty Configuration: 1.5 Inch SMSR Turb. Grid
Reynolds Number: 60000	Reynolds Number: 61742 FSTI: 1.89% Reattachment Point: 80.70%	Reynolds Number: 60645 FSTI: 3.12% Reattachment Point: 80.70%	Reynolds Number: 59233 FSTI: 6.26% Reattachment Point: 69.67%	Reynolds Number: 61666 FSTI: 9.39% Reattachment Point: 69.67%	Reynolds Number: 60236 FSTI: 15.26% Reattachment Point: 60.31%
Reynolds Number: 108000	Reynolds Number: 110525 FSTI: 2.82% Reattachment Point: 69.67%	Reynolds Number: 109550 FSTI: 4.24% Reattachment Point: 69.67%	Reynolds Number: 107857 FSTI: 7.78% Reattachment Point: 64.86%	Reynolds Number: 108605 FSTI: 11.92% Reattachment Point: 69.67%	Reynolds Number: 105772 FSTI: 19.28% Reattachment Point: 64.86%
Reynolds Number: 165000	Reynolds Number: 164910 FSTI: 3.60% Reattachment Point: 64.86%	Reynolds Number: 167528 FSTI: 4.76% Reattachment Point: 64.86%	Reynolds Number: 164713 FSTI: 8.66% Reattachment Point: 64.86%	Reynolds Number: 164551 FSTI: 13.18% Reattachment Point: N/A	Reynolds Number: 162708 FSTI: 19.87% Reattachment Point: N/A

Table 5 shows two more trends. The first is that as the Reynolds number changes from 60,000 to 108,000, the reattachment point moves closer to the leading edge of the blade, and when the Reynolds number increases from 108,000 to 165,000, the reattachment point moves even closer to the leading edge. This trend is shown for the clean configuration of the tunnel as well as each of the dirty configurations. The reattachment point is defined as where the C_p curve returns to its down sloping path just after the plateau (which indicated the separation region). The down sloping trend of the C_p curve is illustrating the reduction in flow velocity over the blade. The

only anomaly in this trend is where most of the anomalies so far have occurred, the high turbulence tests. When comparing data from the test using the 1.5 inch grid at a Reynolds number of 60,000 and the test using the 1.5 inch grid at a Reynolds number of 108,000, an increase in Reynolds number results in the reattachment point moving farther down the suction surface of the blade. This result is contrary to the trends found when comparing data from the other 14 tests. The second trend seen in Table 5 was that as the FSTI increased the reattachment point moved closer to the leading edge of the blade. This was consistent for almost all cases. The one anomaly was found when comparing data between the test using the 0.75 inch grid at a Reynolds number of 108,000 and the test using the 1.0 inch grid at a Reynolds number of 108,000. In this comparison, an increase in FSTI results in the reattachment point moving farther down the surface of the blade, contrary to all 14 of the other test results.

Table 6: Reynolds Number, FSTI, and Bubble Sizes for all 15 tests

Test Matrix	Clean Configuration: No Turbulence Grid	Dirty Configuration: 0.5 Inch SMSR Turb. Grid	Dirty Configuration: 0.75 Inch SMSR Turb. Grid	Dirty Configuration: 1.0 Inch SMSR Turb. Grid	Dirty Configuration: 1.5 Inch SMSR Turb. Grid
Reynolds Number: 60000	Reynolds Number: 61742 FSTI: 1.89% Bubble Size: 41.03%	Reynolds Number: 60645 FSTI: 3.12% Bubble Size: 43.57%	Reynolds Number: 59233 FSTI: 6.26% Bubble Size: 17.74%	Reynolds Number: 61666 FSTI: 9.39% Bubble Size: 18.03%	Reynolds Number: 60236 FSTI: 15.26% Bubble Size: 9.17%
Reynolds Number: 108000	Reynolds Number: 110525 FSTI: 2.82% Bubble Size: 18.30%	Reynolds Number: 109550 FSTI: 4.24% Bubble Size: 18.24%	Reynolds Number: 107857 FSTI: 7.78% Bubble Size: 8.07%	Reynolds Number: 108605 FSTI: 11.92% Bubble Size: 4.81%	Reynolds Number: 105772 FSTI: 19.28% Bubble Size: 4.55%
Reynolds Number: 165000	Reynolds Number: 164910 FSTI: 3.60% Bubble Size: 8.06%	Reynolds Number: 167528 FSTI: 4.76% Bubble Size: 7.32%	Reynolds Number: 164713 FSTI: 8.66% Bubble Size: 6.46%	Reynolds Number: 164551 FSTI: 13.18% Bubble Size: N/A	Reynolds Number: 162708 FSTI: 19.87% Bubble Size: N/A

Table 6 shows two more trends. The first is that as the Reynolds number changes from 60,000 to 108,000 the separation bubble decreases in size and when the Reynolds number increases from 108,000 to 165,000 the separation bubble gets even smaller. This trend is shown for the clean configuration of the tunnel as well as each of the dirty configurations. The separation bubble is defined as the distance between the reattachment point and the separation point. The bubble's size can also be specified by the plateau size in the C_p graph. The second trend from Table 6 was that as the FSTI increased, the separation bubble decreases in size. This was consistent for almost all cases. An anomaly was present, but was only seen on a small scale when comparing individual tests. The anomaly in these comparisons also only occurred in the 60,000 Re tests. It was shown when comparing data between the test using no turbulence grid and the test using the 0.5 inch grid. The anomaly was also seen when comparing the test using the 0.75 inch grid with the test using the 1.0 inch grid. In both of these comparisons, the anomaly showed an increase in FSTI results in a larger separation bubble, which was contrary to the trends shown in the other tests. This is most likely due to the way the separation bubble is calculated. An estimate of where the separation bubble reattaches cannot be interpolated, so it is always assumed that the maximum location for separation is where the bubble reattaches. This method was the most efficient over all 15 tests but did result in two anomalies, contrary to all 14 of the other test results.

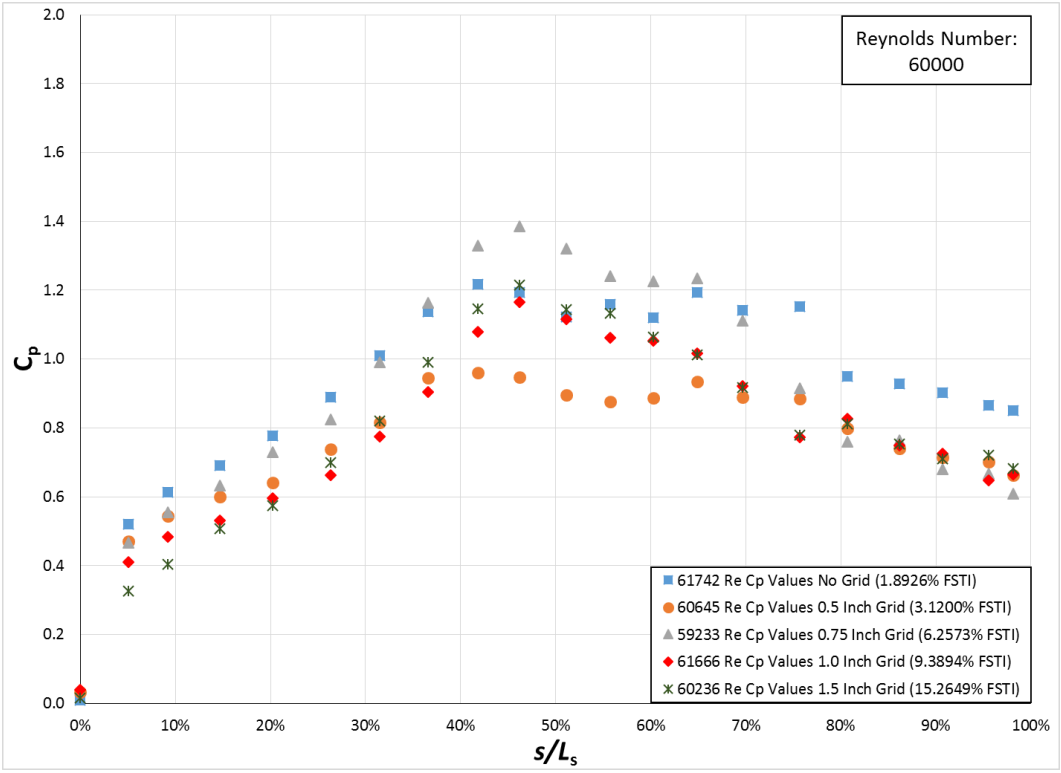
Reynolds Number: 60000
C_P
s/L_s
61742 Re Cp Values No Grid (1.8926% FSTI)
60645 Re Cp Values 0.5 Inch Grid (3.1200% FSTI)
59233 Re Cp Values 0.75 Inch Grid (6.2573% FSTI)
61666 Re Cp Values 1.0 Inch Grid (9.3894% FSTI)
60236 Re Cp Values 1.5 Inch Grid (15.2649% FSTI)

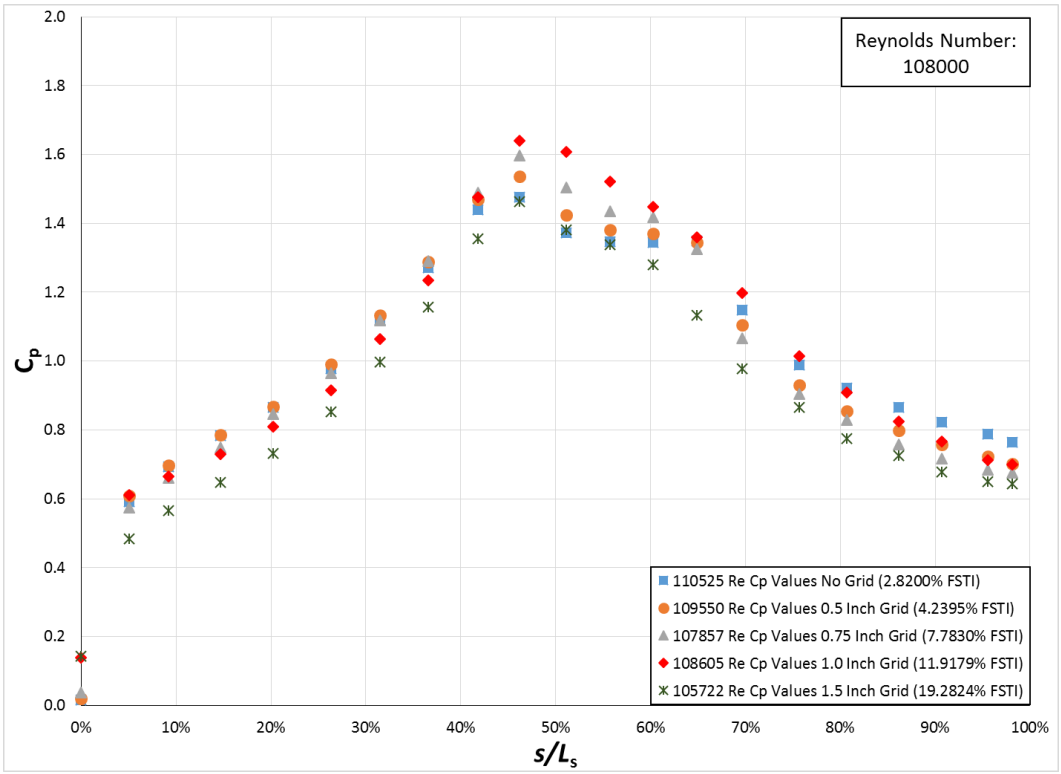
Reynolds Number: 108000
C_P
s/L_s
110525 Re Cp Values No Grid (2.8200% FSTI)
109550 Re Cp Values 0.5 Inch Grid (4.2395% FSTI)
107857 Re Cp Values 0.75 Inch Grid (7.7830% FSTI)
108605 Re Cp Values 1.0 Inch Grid (11.9179% FSTI)
105722 Re Cp Values 1.5 Inch Grid (19.2824% FSTI)

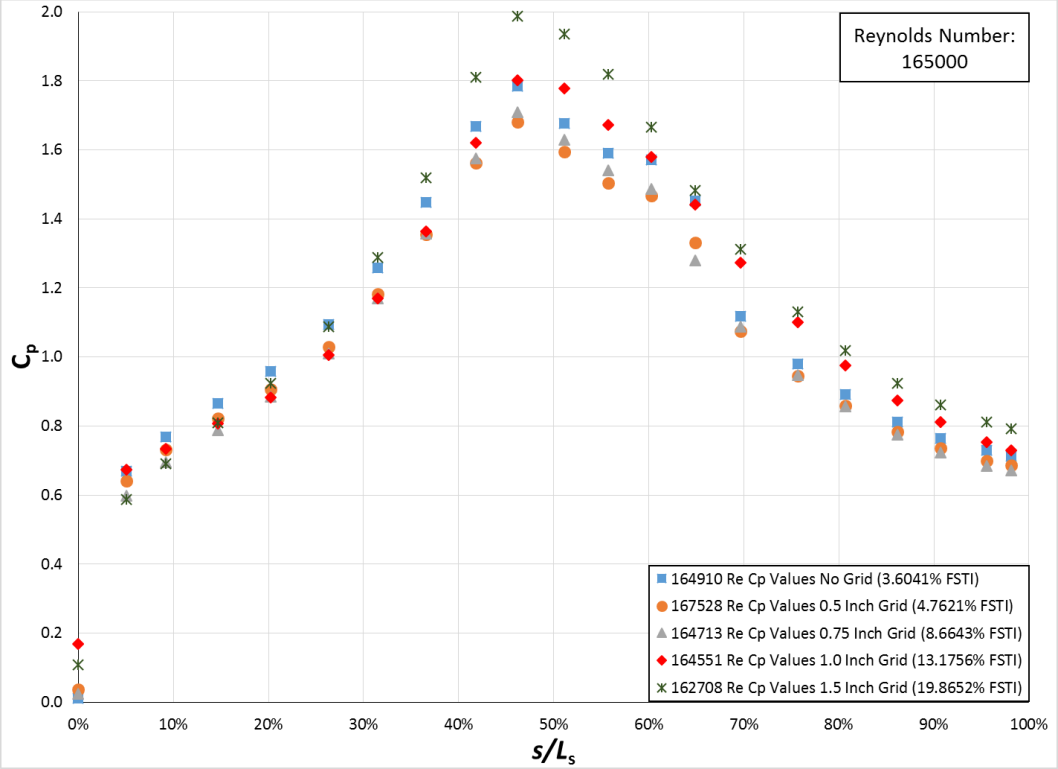

Fig. 8: Coefficient of Pressure Tests Using the Same Reynolds Number while Varying Grids: Read from Top to Bottom - *C_p Graph at 60,000 Re, C_p Graph at 108,000 Re, and C_p Graph at 165,000 Re*

Figure 8 shows the C_p tests when using the different turbulence grid in the tunnel but keeping the Reynolds number constant in the test section. Each graph represents a different Reynold number. The markers represent the C_p's calculated at the 21 pressure ports along the suction surface of the inboard blade. Each of these comparisons show the results of the pressure variations along the blades. The C_p is plotted on the y-axis and the normalized position with respect to the suction surface length, s, is plotted on the x-axis.

The three comparisons in Figure 8 analyze the difference that altering the turbulence intensity has on the coefficients of pressure in the BUC at different Reynolds numbers. After conducting the C_p tests for each of the 15 test conditions and comparing the results, the same trends categorized in Tables 4, 5, and 6 are present.

Conclusion

Through extensive testing in the BUC, the effects that changing FSTI and Reynolds numbers have on the pressure distribution of L1A low-pressure turbine vanes have been studied. Several interesting trends occurring during the generation of turbulence using square-mesh-square-rectangle turbulence grids and the effects of turbulence on pressure distributions were shown. These trends have shown that: an increase in the Reynolds number seen in the test section results

in an increase in FSTI experienced in the test section; FSTI increases at a more rapid rate as the Reynolds number increases at lower Reynolds numbers than it does at higher Reynolds numbers; an increase in the Reynolds number or FSTI results in delayed separation on the suction surface, brings the boundary layer reattachment point closer to the leading edge, and decreases the size of the separation bubble.

Future Work and Recommendations

With turbulence and its effects understood in the BUC, the next step is to investigate the heat transfer. This will be done using liquid crystal thermography in order to analyze the stresses created by flow separation over the L1A test blades. Researching the heat transfer in the separated region is important because turbine blades are thinner at the trailing edge where separation typically occurs and the difference in cooling and heating rates at those locations can induce thermal stresses in the blades, causing them to break prematurely. Once complete for the L1A, the same tests run in this paper and the heat transfer tests using liquid crystals will be run on the L1F blade as well.

Nomenclature

Re	Reynolds Number
ρ	Density of a fluid
V	Velocity of a fluid
L	Characteristic Length of the blade
μ	Dynamic Viscosity of a fluid
P_T	Total Pressure
P_S	Static Pressure
C_p	Coefficient of Pressure

Acknowledgements

The authors would like to express thanks to Dr. Kenneth Van Treuren who is the faculty advisor on this project. Special thanks also go to Mr. Ashley Orr for his help in machining various special parts needed for the research. Thank you also to the ASEE GSW Conference for the opportunity to compete in this contest.

References

[1] "Turbofan," http://en.wikipedia.org/wiki/Turbofan accessed on 4/1/15.

[2] Butler, R. J., Byerley, A. R., Van Treuren, K. W., and Baughn, J. W., 2001, "The Effect of Turbulence Intensity and Length Scale on Low Pressure Turbine Blade Heat Transfer," International Journal of Heat and Fluid Flow, 22, pp. 123-133.

[3] Pharris, T. M., Hirst, O. E., and Van Treuren, K. W., 2015, "Effects of Flow Separation on a Highly Loaded, Low-Pressure Gas Turbine Blade at Low Reynolds Numbers," IMECE2015-54167. 2015 International Mechanical Engineering Congress and Exposition. Houston, TX.

[4] Becker, J., Bond, G., Fox, J., and Sapp, K., 2011, "Measuring Flow Separation and Effects of Deposition on a Gas Turbine Blade," Mechanical Engineering Laboratory, Baylor University, Waco, TX.

[5] Hawkins, M., Lopez, B., Camp, J., Lagat, J., Martin, E., Massingill, A., Burgess, A., Davis, K., and Mart, S., 2009, "Turbine Cascade Facility Final Report," Electromechanical Systems, Baylor University, Waco, TX.

[6] Roach P. E., 1986, "The Generation of Nearly Isotropic Turbulence by Means of Grids," International Journal of Heat and Fluid Flow, Volume 7, Issue 2. Pp. 117-125